Journal Pre-proofs

Sonochemical synthesis and anchoring of zinc oxide on hemin-mediated multiwalled carbon nanotubes-cellulose nanocrystals nanocomposite for ultra-sensitive detection of H_2O_2

Selvakumar Palanisamy, Vijayalakshmi Velusamy, Sridharan Balu, Sethupathi Velmurugan, Thomas C.K. Yang, Shih-Wen Chen

PII: S1350-4177(19)31810-3
DOI: https://doi.org/10.1016/j.ultsonch.2019.104917
Reference: ULTSON 104917

To appear in: *Ultrasonics Sonochemistry*

Received Date: 13 November 2019
Revised Date: 27 November 2019
Accepted Date: 2 December 2019

Please cite this article as: S. Palanisamy, V. Velusamy, S. Balu, S. Velmurugan, T.C.K. Yang, S-W. Chen, Sonochemical synthesis and anchoring of zinc oxide on hemin-mediated multiwalled carbon nanotubes-cellulose nanocrystals nanocomposite for ultra-sensitive detection of H_2O_2, *Ultrasonics Sonochemistry* (2019), doi: https://doi.org/10.1016/j.ultsonch.2019.104917

Sonochemical synthesis and anchoring of zinc oxide on hemin-mediated multiwalled carbon nanotubes-cellulose nanocrystals nanocomposite for ultra-sensitive detection of H_2O_2

Selvakumar Palanisamy[a*], Vijayalakshmi Velusamy[b*], Sridharan Balu[c], Sethupathi Velmurugan[c], Thomas C.K. Yang[a, c, *], Shih-Wen Chen[c]

[a]Center of Precision Analysis and Material Research, National Taipei University of Technology, Taipei, Taiwan (ROC).

[b]Division of Electrical and Electronic Engineering, Manchester Metropolitan University, Chester Road, Manchester, United Kingdom.

[c]Department of Chemical Engineering and Biotechnology, National Taipei University of Technology, Taipei, Taiwan (ROC).

*Corresponding authors: prmselva@gmail.com (S. Palanisamy); V.Velusamy@mmu.ac.uk (V. Velusamy); ckyang@mail.ntut.edu.tw (T.C.K. Yang).

Abstract

In this work, the metal oxide and biopolymer nanocomposites on multiwalled carbon nanotubes (MWCNT) were prepared using a simple sonochemical method. The hexagonal nanorods of zinc oxide (ZnO NR) were synthesized by probe sonication (frequency = 20 kHz, amplitude = 50) method and were integrated on ultrasonically functionalized MWCNT-cellulose nanocrystals (MWCNT-CNC) for the first time. The stable hemin bio-composites also were prepared using the bath sonication (37 kHz of frequency, 150 W of power) method, and was used for the selective and ultrasensitive electrochemical detection of H_2O_2. The UV-Vis spectroscopy studies confirmed the presence of native hemin on MWCNT-CNC/ZnO NR nanocomposite. Cyclic voltammetry studies revealed that an enhanced redox electrochemical behaviour of hemin was observed on hemin immobilised MWCNT-CNC/ZnO NR nanocomposite than that of other hemin modified electrodes. Also, the MWCNT-CNC/ZnO NR/hemin modified SPCE showed 2.3 folds higher electrocatalytic activity with a lower reduction potential (-0.2 V) towards H_2O_2 than that of other investigated hemin modified electrodes including hemin/MWCNT and hemin/CNC-ZnO. The fabricated biosensor displayed a stable amperometric response (-0.2 V vs Ag/AgCl) in the linear concentration of H_2O_2 ranging up to 4183.3 µM with a lower detection limit of 4.0 nM.

Keywords: Sonochemical synthesis; Screen-printed carbon electrode; Electrocatalysis; Selectivity; Sensitivity; Biosensor

1. Introduction

The cost-effective fabrication of highly sensitive electrochemical biosensors has become a hot topic in recent years to the researchers due to their vital role in the detection of various organic, inorganic, bio-molecules, pollutants, and heavy metals [**1, 2**]. Among, the qualitative and quantitative measurement of H_2O_2 in pharmaceutical and food industries has paid much attention due to its critical importance, chemical property, and harmful nature to the human health and environment [**3**]. Owing to the oxidative and antibacterial properties of H_2O_2, it has been primarily used as an oxidiser in organic reactions, bleaching agent in the paper industry, an antiseptic agent in pharmaceutical industries [**4, 5**]. Various type of methods has been reported for real-time quantification of H_2O_2 [**6-8**], yet the electrochemical methods have been profound in the real-time quantification of H_2O_2 due to their distinct advantages [**9**]. To date, a range of sensors utilising either enzymatic or non-enzymatic has been reported for detection of H_2O_2 [**10–12**]. The enzyme-based biosensors are highly selective towards H_2O_2, but the complicated enzyme immobilisation procedures and less stability of the adsorbed enzymes make them less attractive. Similarly, the non-enzymatic H_2O_2 sensors have more advantages such as easy preparation, highly stable and cost-effective, yet these sensors are not highly selective as enzyme-based biosensors. To address the above limitations, the development of stable and selective H_2O_2 sensors is more important to various practical applications. Recent studies revealed that hemin (iron protoporphyrin) had been used as an alternative enzyme mimic for heme redox proteins based H_2O_2 biosensors due to its high stability, commercial availability, close relative nature (similar redox-active centre) and peroxidase-like activity to H_2O_2 [**13–16**]. Hitherto, different kind of materials has been employed as a support for the immobilisation of hemin such as carbon nanomaterials [**16, 17**], inorganic/organic polymer materials [**13**], metal and metal alloy nanoparticles [**15**].

Multiwalled carbon nanotubes (MWCNT) has shown its enormous usage in the fabrication of stable electrochemical sensors and biosensors. Also, MWCNT has exceptional physicochemical properties that pave the pathway to the excellent electron promotion ability of immobilised enzymes on MWCNT [**20**]. However, MWCNT possesses a low dispersion ability in many aqueous solvents which limits its usage in practical applications [**21**]. In order to address the issue, the acid functionalization MWCNT or composite with other nanomaterials have been used to increase the dispersion ability of MWCNT [**22, 23**]. Compared to acid functionalization of MWCNT, the functionalization with other nanomaterials is more environmentally friendly and less tedious route. The multiple rolled graphene layer structure of MWCNT is more beneficial to functionalization with nanomaterials such as graphenoids, carbohydrate polymers, organic polymers and metal oxides [**23–25**]. Among different nanomaterials, cellulose nanocrystals (CNC) is one of the

nanoforms of cellulose carbohydrate polymer and has excellent biodegradability, superior mechanical strength, abundant surface reactive sites and excellent film-forming ability with other materials including MWCNT [**26, 27**]. The introduction of CNC on MWCNT could improve the physicochemical properties of both nanomaterials and also improves the dispersion ability of MWCNT into the CNC aqueous solution since CNC can be easily dispersed in water via hydrogen bonding. On the other hand, zinc oxide (ZnO) is well-known semiconductor material, has higher surface activity with excellent stability and biocompatibility [**28**]. To date, different form of nano ZnO (nanoparticles, nanorods, nanobows, nanobelts, nanowires) has been synthesized by thermal evaporation, hydrothermal and chemical solution deposition [**28, 29**]. Sonochemical methods have been widely used to prepare different nanostructures of metal and metal alloy nanoparticles [**30, 31**]. Also, the ultrasound-assisted synthesis has been used to accelerate the rate of reaction and improved the yield and reproducibility of nanomaterials and its dispersions [**30**]. Hence, a simple ultrasound-assisted method is used for synthesis of ZnO nanorods (NR) and preparation of highly stable MWCNT-CNC composite. Recent studies show that nano and microstructures of ZnO have been widely functioned as a suitable matrix for immobilising of enzymes and proteins including glucose oxidase and heme proteins [**32–34**]. Also, the composites of ZnO with other materials also been utilized for the fabrication of non-enzymatic sensors for glucose and H_2O_2 [**35–37**]. However, in this work, the fascinating properties of MWCNT-CNC and ZnO NR have been combined with hemin using a simple sonochemical method, and as-prepared nanocomposite is used for H_2O_2 biosensor applications. Also, the direct combination of ZnO NR with either CNC or MWCNT-CNC has not been reported yet, and their related application to the biosensors are still limited.

In this research, a simple solution based sonochemical synthesis of novel bio-composite of MWCNT-CNC/ZnO NR/hemin was reported. The as-prepared MWCNT-CNC/ZnO NR/hemin bio-composite electrode was further used as an enhanced biosensor matrix for real-time electrochemical quantification of H_2O_2. The electrochemical redox behaviour and electron-transfer properties of MWCNT-CNC/ZnO NR/hemin composite modified SPCE was compared with MWCNT-CNC/hemin, and CNC-ZnO NR/hemin modified SPCEs and discussed briefly. The selectivity, operational stability and practicality of the MWCNT-CNC/ZnO NR/hemin composite was also examined and discussed. The analytical advantages of the as-prepared biosensor were compared with reported hemin immobilized graphene and carbon nanotubes composite based H_2O_2 biosensors.

2. Experimental

2.1. Materials and methods

Cellulose microfiber (medium from Cotton linters), Multiwalled carbon nanotubes (12-30 nm outer diameter), zinc nitrate hexahydrate ($Zn(NO_3)_2.6H_2O$), NaOH, H_2O_2 (30%), hemin chloride (≥90.0% assay, from bovine), H_2SO_4, ascorbic acid and all other chemicals utilized in this research were acquired from Sigma-Aldrich. The screen-printed carbon electrodes of model SE101 (0.071 cm^2 geometric surface area) were purchased from the Zensor R&D corporation in Taiwan. 0.1 M stock solutions of Na_2HPO_4 and NaH_2PO_4 were used for the preparation of pH 7.0 on dilution with doubly distilled (DD) water, and the pH of the solutions was adjusted using 0.1 M sulfuric acid or 0.1 M sodium hydroxide solutions. The low-fat milk was purchased from the local market in Taipei.

The crystalline patterns of the composite materials were determined by Panalytical X'pert pro with X-ray wavelength of 1.54060Å (Cu-Kα). The voltammetric and amperometric assessments were analyzed by CHI1211C CH instruments (USA). The broader Fourier-transform infrared spectral data in the range of 400-4000 cm^{-1} from the PerkinElmer Frontier spectrophotometer and Dongwoo 500i model spectrophotometer was employed to record the Raman spectrum of the as-prepared nanocomposites. The UV-Vis absorbance spectrum was recorded on Agilent technology-Cary5000 UV-Vis spectrophotometer. The surface micrographs and elemental analysis of the nanocomposites were obtained from JSM-7610F, JEOL field emission scanning electron microscopy (FE-SEM). For the probe sonication, the Misonix S-4000 model microtip probe sonicator (50 as amplitude, pulse ON and OFF = 3-sec) and for bath sonication Elmasonic Easy 60H model bath sonicator (37 kHz frequency, 150 W power) were used. The electrochemical measurements were performed in a deoxygenated electrolyte solution (N_2 atmosphere) at 25 ± 2 ºC. The modified SPCE was used as a working electrode, and reference and counter electrodes were Pt wire and Ag/AgCl (with saturated KCl) respectively.

2.2. Synthesis of MWCNT-CNC/ZnO NR nanocomposite

The CNC was prepared by sonication under mechanical string using Misonix S-4000 model microtip probe sonicator (20 kHz frequency, 50 as amplitude) where the solution containing cellulose microfibers (CMF) with 65% H_2SO_4 for 45 min. Then, the suspension diluted with a copious amount of DD water and washed and centrifuged until the pH 7.0 reached. The obtained CNC were dried and re-dispersed into the DD water using sonication about 30 min. For the preparation of MWCNT-CNC composite, the pristine MWCNT (2 mg mL^{-1}) was added into CNC suspension. The above mixture was bath sonicated in Elmasonic Easy 60H model ultrasonicator (37 kHz frequency, 150 W power) over 30 min to

obtain the stable dispersion of MWCNT-CNC composite (see **Scheme 1**). Then, the zinc oxide precursors ($Zn(NO_3)_2.6H_2O$ and NaOH) were added into the MWCNT-CNC dispersion, and the mixture was probe sonicated for a min using the Misonix S-4000 model microtip probe sonicator (20 kHz frequency, 50 as amplitude). The obtained mixture was placed in a hot plate over 4 h at 70 ºC. The final composite was separated using centrifugation after rinsing with DD water and absolute ethanol. The obtained material is named as MWCNT-CNC/ZnO NR nanocomposite and was dried at 80 ºC for overnight. The same method was used for the preparation of ZnO and CNC/ZnO without the addition of MWCNT-CNC and MWCNT. The as-synthesized composite (2 mg mL^{-1}) was added into the DD water, and its dispersions were prepared using sonication about 30 min.

About 10 mg of hemin chloride was added into the 2 mL of the MWCNT-CNC/ZnO NR composite dispersion and bath sonicated (37 kHz frequency, 150 W power) for 30 min. The resulting MWCNT-CNC/ZnO NR/hemin composite dispersion was further used for the electrode modifications. The schematic depiction for the preparation of MWCNT-CNC/ZnO NR nanocomposite and MWCNT-CNC/ZnO NR/hemin composite is shown in **Scheme 1**. For comparison, CNC/ZnO/hemin, MWCNT-CNC/hemin and pristine MWCNT/hemin solutions were also prepared using the above-mentioned methodology. The obtained solutions were stored at room temperature unless otherwise stated.

2.3. Preparation of biosensor

For the electrode preparations, about 8 µL of MWCNT-CNC/ZnO NR/hemin composite dispersion was cast on unmodified SPCE and dried at 50 ºC. For the comparative studies, CNC/ZnO NR/hemin/SPCE, MWCNT-CNC/hemin/SPCE, MWCNT/hemin/SPCE, hemin/SPCE, and MWCNT/SPCE were prepared by casting 8 µL of CNC/ZnO NR/hemin, MWCNT-CNC/hemin and MWCNT/hemin, hemin, and pristine MWCNT dispersions on unmodified SPCEs and oven-dried at 50 ºC. The as-prepared electrodes were used for the voltammetric and amperometric studies and were stored at room temperature (25 ± 2 ºC) in dry condition.

3. Results and discussion

3.1. Characterisations

The surface micrographs of the as-synthesized different materials were analysed using high-resolution FE-SEM. The FESEM image of pristine MWCNT (**Fig. 1A**) appears as smooth and uniform tubes like morphology with a diameter of 20 ± 6 nm. The FESEM image of CNC (**Fig. 1B**) appears as aggregated ultra-small microcrystals morphology with a diameter of 44 nm. On the other hand, the surface morphology

of untreated CMF appeared as ultra-small fiber morphology (**Fig. 1B** inset), as reported early [**38**]. **Fig. 1C** reveals the surface morphology of MWCNT-CNC composite where the CNC (blue arrow) was observed and anchored on the surface of MWCNT (yellow arrow). The FESEM image of CNC/ZnO composite (**Fig. 1D**) confirms the presence of CNC on the flat rod-like structure of ZnO. The average diameter of ZnO NR was 90 ± 8 nm with an average length of 1.6 μm with hexagonal symmetry. The surface morphology of MWCNT-CNC/ZnO NR nanocomposite (**Fig. 1E**) reveals the presence of CNC and ZnO NR (black arrow) on the surface of MWCNT. It is thought-provoking to note that the diameter and lengths of CNC and ZnO NR on MWCNT were found similar to **Fig. 1B** and **C**. The successful formation of MWCNT-CNC/ZnO NR nanocomposite were confirmed by the abovementioned discussions. One can easily be seen from **Fig. 1F** that a thin layer of hemin (light blue arrow) was visible and uniformly covered the surface of MWCNT-CNC/ZnO NR nanocomposite, which further confirms the presence of hemin on the nanocomposite. The EDS of the MWCNT-CNC/ZnO NR/hemin composite is shown in **Fig. 1G**. Clear EDX signals were observed for carbon (49.9 wt.%), oxygen (16.3 wt.%), zinc (32.7 wt.%) elements which confirmed the presence of MWCNT-CNC and ZnO. Also, a noticeable EDX signal was observed for the presence of iron and chloride on MWCNT-CNC/ZnO NR/hemin composite, which assures the existence of hemin chloride on the MWCNT-CNC/ZnO NR nanocomposite. From the above evidence confirmed the formation of MWCNT-CNC/ZnO NR nanocomposite and MWCNT-CNC/ZnO NR/hemin composite.

The crystalline nature of as-synthesized composite materials was examined by XRD. The XRD patterns of MWCNT (a), CNC/ZnO NR (b) and MWCNT-CNC/ZnO NR/hemin (c) are shown in **Fig. 2A.** The pristine MWCNT show the diffraction peaks with a 2θ value of 26.1º, 42.5º, 43.7º, 53.6º and 77.6º which are indexed to the (002), (100), (101), (004), (110) crystal planes of MWCNT. The CNC-ZnO composite shows diffraction peaks at 31.8º, 34.5º, 36.4º, 47.5º, 56.6º, 63º, 66.4º, 67.8º, and 69.1º are corresponding to the planes of the hexagonal phase ((100), (002), (101), (102), (110), (103), (200), (112), and (201)) of ZnO. Also, CNC-ZnO composite shows diffraction peak at 17.6º and 22.6º which are corresponding to (101) and (002) planes of cellulose. Other diffraction peaks in CNC-ZnO composite are related to the utilised substrate. The similar diffraction patterns were observed on MWCNT-CNC/ZnO NR nanocomposite which confirms the existence of MWCNT and CNC-ZnO. The FT-IR spectrum of hemin adsorbed MWCNT-CNC/ZnO NR nanocomposite (**Fig. 2B**) shows the characteristic absorption bands for hemin at 1570-1600 cm^{-1} which is due to the strong stretching of the benzenoid ring. Also, the stretching vibrations of the pyrrole group appeared at 1100-1200 cm^{-1}. The result confirmed the presence of hemin on the nanocomposite. The cellulose nanocrystals show the strong distinctive peaks at 890-903 cm^{-1} which represents the β-

glycosidic linkages. The stretching vibrations of C–O–C pyranose ring appeared at 1054 cm^{-1}, and the absorption vibration bands at 1375-1383, 1420-1432, 1632-1650 cm^{-1} are attributed to the CH_2 wagging, CH_2 scissoring, O–H bending by the adsorbed water respectively. The results confirmed the successful formation of MWCNT-CNC/ZnO NR/hemin nanocomposite. It is considered to refer that for the pristine MWCNT shows a significant peak at 1634 cm^{-1} which is corresponding to the C═C stretching vibrations. Furthermore, in the FT-IR spectrum of ZnO shows the significant bands at 455-545 cm^{-1} and 3230-3265 cm^{-1} are specifying the stretching vibrations of ZnO and O–H stretching by the adsorbed water molecules respectively. The results concluded that the FT-IR spectrum of ZnO and MWCNT are consistent with the FT-IR spectrum of MWCNT-CNC/ZnO NR nanocomposite. Moreover, the formation of MWCNT-CNC/ZnO NR nanocomposite was further confirmed by the Raman spectroscopy studies, and the representative Raman spectrum of pristine MWCNT, MWCNT-CNC and MWCNT-CNC/ZnO NR nanocomposite is shown in **Fig. 2C.** The moderated D band at 1300∼1400 cm^{-1} in the Raman spectrum of MWCNT is due to the high degree of disorder of graphite. Also, another sharp and intense G band was observed at 1500∼1600 cm^{-1} and are because of the tangential vibrational mode of MWCNT. The MWCNT-CNC and MWCNT-CNC/ZnO NR composites show the broadband at 1010-1180 cm^{-1} which is representative band from utilised CNC. It is interesting to note that the MWCNT-CNC and MWCNT-CNC/ZnO NR nanocomposite shows similar peak position for D and G bands, which indicates that the nature of MWCNT remains same in the nanocomposite. The intensity ratio (I_D/I_G) of MWCNT-CNC/ZnO NR (0.31) and MWCNT-CNC (0.28) is higher than pristine MWCNT (0.2). Here, the increase in the I_D/I_G is on account of the occupancy of more oxygen defects at MWCNT from ZnO NR and CNC. Therefore, the results confirm the existence of surface defects on nanocomposite than pure MWCNT. The presence of hemin on the nanocomposite was further confirmed using UV-Vis spectroscopy since it is used to confirm the sharp absorption band of hemin. **Fig. 2D** shows UV-Vis spectra of CNC/ZnO NR (a), MWCNT-CNC (b), MWCNT-CNC/ZnO NR/hemin (c) and pristine hemin (d). ZnO NR shows a strong absorption edge at 369 nm and is higher than reported value (358 nm) for bulk ZnO [**28**]. The UV-Vis spectrum of MWCNT-CNC shows a broad absorption band around 280-310 nm which is associated to the π-π* transition of the benzenoid rings of MWCNT and CNC. The native hemin shows a sharp absorption peak around 386 nm which is because of the presence of monomeric hemin hydroxide on hemin [**13**]. On the other hand, the Soret band of hemin is redshifted on the UV-Vis spectrum of MWCNT-CNC/ZnO NR/hemin nanocomposite which is possibly due to the strong attraction of hemin with ZnO NR and MWCNT-CNC. The above results further confirmed the formation of MWCNT-CNC/ZnO NR/hemin nanocomposite.

3.2. Electrochemical redox behaviour of hemin

The electrochemical redox behaviour of hemin modified different electrodes were investigated using cyclic voltammetry. Cyclic voltammetry is widely used as an ideal method for studying the electrochemical redox activity of immobilized enzyme or enzyme mimics. The cyclic voltammetric response of different hemin modified and unmodified SPCEs in pH 7.0 at a scan rate of 100 mV/s are shown in **Fig. 3A.** Usually, the electrochemical redox behaviour of hemin is associated with the oxidation and reduction of Fe^{II}/Fe^{III} redox-active centre of immobilised hemin [**13**]. Compared to the reduction peak current (I_{pc}) of hemin/SPCE (a) and CNC/ZnO NR/hemin/SPCE (b), the MWCNT/hemin (c) and MWCNT-CNC/hemin (d) show the enhanced I_{pc} with lower reduction potential for hemin. The cathodic peak potential (E_{pc}) of hemin on MWCNT/hemin and MWCNT-CNC/hemin modified SPCEs appeared at -0.332, and -0.346 V, respectively. However, these investigated electrodes did not show apparent reversible oxidation peak of hemin, which reveals that the direct electron nature of hemin is hindered on these modified electrodes. However, MWCNT-CNC/ZnO NR modified SPCE show a well-defined reversible couple, and the corresponding E_{pa} and E_{pc} appeared at -0.336 and 0.283 V. Also, about 53 mV was calculated as the peak to peak separation (ΔE_p) for the hemin redox couple. The obtained ΔE_p is much smaller than reported hemin, hemin/graphene-polypyrrole and hemin/graphene-modified electrodes [**13**], which authenticates the superior direct electrochemistry of hemin on the nanocomposite. Also, the observed I_{pc} was 2.7 and 3.3 folds higher than MWCNT/hemin, and MWCNT-CNC/hemin modified SPCEs, which indicating the enhanced electron transfer of hemin on MWCNT-CNC/ZnO NR composite. The direct electrochemical behaviour of hemin only is observed when incorporating the MWCNT-CNC with ZnO NR, which reveals that the MWCNT-CNC/ZnO NR nanocomposite provides a suitable microenvironment for entrapping the hemin molecule on the electrode surface. The unique biocompatible nature of CNC can easily attract the hemin molecules via hydrogen bonding and the ZnO NR acts as an interconnecting material for adsorption of more hemin molecule on MWCNT-CNC and provides a suitable microenvironment for the adsorbed hemin molecules. Also, the high conducting nature of MWCNT improves the electron transfer and direct electrochemistry of adsorbed hemin towards the electrode surface. The above results confirmed that MWCNT-CNC/ZnO NR nanocomposite is more suitable for fabrication of hemin biosensor than MWCNT-CNC with CNC/ZnO NR nanocomposites. In order to verify the electron transfer properties of different modified electrodes without hemin, the cyclic voltammetric response of MWCNT-CNC/ZnO NR, CNC/ZnO, MWCNT-CNC and pristine MWCNT modified SPCEs were investigated in 5 mM potassium ferricyanide with 0.1 M KCl at a scan rate of 100 mV/s. **Fig. 3B** reveals that a clear redox couple (related to $Fe(CN)_6^{3-}$

/$Fe(CN)_6^{4-}$) has appeared for all the modified SPCEs. The ΔE_p of the redox couple was calculated as 120, 161, 115 and 136 mV for MWCNT-CNC/ZnO NR, MWCNT-CNC, pristine MWCNT and CNC/ZnO modified SPCEs, respectively. Also, the MWCNT-CNC/ZnO NR modified SPCE shows 1.5 and 2.3 folds enhanced current response to ferricyanide redox couple than that of MWCNT-CNC and pristine MWCNT modified SPCE. The result confirmed that MWCNT-CNC/ZnO NR modified electrode has faster electron transfer characteristics with improved electrochemical activity than other investigated modified electrodes.

The electrochemical redox behaviour of MWCNT-CNC/ZnO NR/hemin modified electrode was further studied by cyclic voltammetry with varying scan rates (50 to 500 mV/s). The obtained cyclic voltammetry results are shown in **Fig. 4A**. The I_{pa} and I_{pc} of hemin redox couple were linearly increasing with the scan rates, and they were linearly proportional to the scan rates from 50 to 500 mV. The result confirmed that the direct electrochemistry of hemin on MWCNT-CNC/ZnO NR nanocomposite is a surface-controlled electrochemical process. The Laviron's equation (1) was used to calculate the average surface coverage (Γ*) of hemin on MWCNT-CNC/ZnO NR nanocomposite.

$$Ip = \frac{n^2F^2\nu\Gamma^* A}{4RT} \qquad (1)$$

Where v = scan rate (mV/s), n = electron transfer number of hemin (n=1), A = active electrode surface area of the hemin modified electrode and F = Faraday constant (C mol^{-1}). The calculated Γ* value is 1.33×10^{-8} mol cm^{-2} and was higher than theoretical monolayer coverage of hemin (7.0×10^{-11} mol cm^{-2}) and previously reported hemin modified electrodes. Also, the Laviron's equation is used to calculate the heterogeneous electron transfer rate constant (K_s) of hemin on MWCNT-CNC/ZnO NR.

$$\log K_s = \alpha\log(1-\alpha) + (1-\alpha)log\alpha - log\frac{RT}{nF\nu} - (1-\alpha)\alpha\frac{nF\Delta E_p}{2.3RT} \qquad (2)$$

Where ΔE_p = peak to peak separation of the hemin redox couple, n is equal to 1 (electron transfer of hemin), and α (charge transfer coefficient) is assumed to be 0.5. The K_s of hemin on MWCNT-CNC/ZnO NR nanocomposite is calculated to be 6.96 s^{-1} and was much higher than hemin based graphene composite modified electrodes [**13, 38, 39**]. The result confirmed the faster electron transfer kinetics of adsorbed hemin towards the electrode surface. It is well-known that the electrochemical behaviours of hemin and other redox-active biomolecules are pH-dependent. Hence, the effect of pH concerning the electrochemical redox behaviour of MWCNT-CNC/ZnO NR/hemin modified electrode was studied, and the results are shown in **Fig. 4C**. The MWCNT-CNC/ZnO NR/hemin modified electrode shows well-defined redox couple of hemin in the pH 3.0, 5.0, 7.0 and 9.0. From the results, one can conclude that notable changes of iron ligation in the protoporphyrin macrocycle at various pH. The plot of E_{pa} and E_{pc} of hemin

redox couple is found linear to the pH from 3.0-9.0, and the correlation coefficients are 0.998 and 0.995 (**Fig. 4D**). Also, the slope is found to be 53.6 mV per unit pH, and the value was close to the reported theoretical value (59 mV/pH) for the number of protons transferred accompanied by an equal number of electrons for the reversible systems. The result also implies that the equal number of protons and electrons are effectively participating in the redox electrochemical reaction of hemin on the nanocomposite towards electrode surface. The mechanism related to the redox electrochemical behaviour of hemin on various modified electrodes is well documented and discussed, and the electrochemical redox behaviour of hemin is associated with the single electron transferred redox reaction on the electrode surface [**39**].

3.3. Electrocatalytic activity of hemin modified electrodes

In order to prove the high catalytic activity of MWCNT-CNC/ZnO NR/hemin nanocomposite, the cyclic voltammetric response of hemin modified different electrodes was investigated. The electrocatalytic activity of MWCNT-CNC/ZnO NR/hemin/SPCE was compared with the hemin/SPCE, MWCNT-CNC/hemin/SPCE and CNC/ZnO NR/hemin/SPCE. The cyclic voltammetry experiments were performed in a 1.2 mM H_2O_2 containing deoxygenated pH 7.0 and are displayed in **Fig. 5A**. The hemin and CNC/ZnO NR/hemin modified SPCEs show an E_{pc} to H_2O_2 at -0.283 and -0.431 V. While, the E_{pc} of H_2O_2 observed on MWCNT-CNC/hemin at -0.252 and the observed E_{pc} was 31 and 179 mV lower than those observed at hemin/SPCE and CNC/ZnO NR/hemin/SPCE. The result shows that the MWCNT-CNC/hemin electrode has a lower E_{pc} to H_2O_2 and is possibly from the MWCNT and CNC. However, the I_{pc} of MWCNT-CNC/hemin electrode was found similar to CNC/ZnO NR/hemin electrode. On the other hand, MWCNT-CNC/ZnO NR/hemin nanocomposite modified electrode shows an enhanced E_{pc} at -0.206 V. The I_{pc} of the response at -0.206 V was 3 folds higher than CNC/ZnO NR/hemin, and MWCNT-CNC/hemin modified electrodes. Also, the E_{pc} of H_2O_2 was 46 mV lower than MWCNT-CNC/hemin modified electrode. The obtained electrocatalytic activity (current response and potential) of hemin immobilised different electrodes towards a reduction of H_2O_2 is plotted in **Fig. 5B**. The comparative results revealed that the MWCNT-CNC/ZnO NR/hemin nanocomposite modified electrode has higher reduction capability with lower E_{pc} towards H_2O_2 than other hemin modified electrodes. The fascinating properties of ZnO NR (higher surface to volume) with MWCNT-CNC (high conductivity and biocompatibility) are resulting in the enhanced electrocatalytic activity of the fabricated biosensor towards H_2O_2.

The cyclic voltammetry was used to study the electrocatalysis of H_2O_2 using MWCNT-CNC/ZnO NR/hemin nanocomposite modified electrode, and the obtained results are shown in **Fig. 5C**. In the

absence of H_2O_2 (curve a'), MWCNT-CNC/ZnO NR/hemin nanocomposite exhibits a redox couple which is due to presence of Fe redox-active centre in hemin. Whereas, an additional reduction peak at -0.138 V was observed upon addition of 0.2 mM H_2O_2 and increased with further additions (0.7 and 1.2 mM) of H_2O_2. The I_{pc} of H_2O_2 on MWCNT-CNC/ZnO NR/hemin nanocomposite modified electrode had a linear dependence with different concentrations of H_2O_2, and a correlation coefficient is 0.9983 (**Fig. 4D**). Also, E_{pc} of hemin had notable shift and increases when increasing the concentration of H_2O_2, and the E_{pa} of hemin almost disappeared. The result indicates the typical electrocatalysis of H_2O_2 by hemin redox couple. A plausible mechanism for electrochemical reduction of H_2O_2 by hemin redox couple on MWCNT-CNC/ZnO NR nanocomposite modified electrode is shown **Scheme 2**.

3.4. Determination of H_2O_2

The amperometric *i-t* method has been employed to quantify the H_2O_2 since it is an effective method to determine H_2O_2 using redox-active enzyme-modified electrodes. **Fig. 6A** shows a typical current-time response of MWCNT-CNC/ZnO NR/hemin nanocomposite modified SPCE for additions of various concentration H_2O_2. Pure N_2 gas was purged (10 min) into the electrolyte solution (pH 7.0) to remove the oxygen molecule from the electrolyte solution. The applied potential about -0.2 V was used for the current-time measurements of the biosensor. In the absence of H_2O_2, no apparent response was observed on MWCNT-CNC/ZnO NR/hemin nanocomposite modified SPCE, and only a stable background signal was observed. Whereas, for the addition of 1, 5, 25, 75 and 150 μM H_2O_2, a good amperometric response was observed on MWCNT-CNC/ZnO NR/hemin nanocomposite modified electrode. The MWCNT-CNC/ZnO NR/hemin nanocomposite modified electrode even show a good response for 10 and 100 nM addition of H_2O_2 (**Fig. 6A inset**). The response time of the fabricated biosensor towards the detection of H_2O_2 is 2 s, which demonstrates that fast electro-reduction of H_2O_2 on MWCNT-CNC/ZnO NR/hemin nanocomposite. The observed current response vs. concentration of H_2O_2 is plotted and was found linear up to 4183.3 μM with a correlation coefficient 0.998 (**Fig. 6B**). The limit of detection (LOD) is calculated as 0.004 μM with the sensitivity of 0.134 $\mu A \mu M^{-1}$. The obtained electrochemical and electroanalytical results of MWCNT-CNC/ZnO NR/hemin nanocomposite electrode was further compared with other recently reported hemin and hemoglobin modified nanomaterials based biosensors. The comparative results (working potential, LOD, linear response range and K_s) are summarised in **Table 1**. It is well evident that the working potential and LOD is much lower than other biosensors reported early. Also, the biosensor shows superior linear response range and K_s than reported hemin modified graphene and multiwalled carbon nanotubes based

biosensors in **Table 1** [**13, 14, 16, 17, 38–44**]. The results confirmed that MWCNT-CNC/ZnO NR/hemin nanocomposite could be used for more extensive detection of H_2O_2 in its low levels.

The selectivity of MWCNT-CNC/ZnO NR/hemin nanocomposite was examined for the sensing of H_2O_2 among the other interfering compounds, including electroactive biomolecules. **Fig. 6C** shows the selectivity related to the amperometric response of MWCNT-CNC/ZnO NR/hemin nanocomposite electrode for addition of H_2O_2 (a) and positive and negative metal ions (Ni^{2+} (b), Mg^{2+} (c), Ca^{2+} (d), Cl^- (e), SO_4^{2-} (f), SO_3^{2-} (g) and PO_4^{3-} (h)) and biomolecules (glucose (i), ascorbic acid (j), epinephrine (k), dopamine (l), uric acid (m) and l-cysteine (n)) in pH 7.0 (E_{app} = -0.2 V). The addition of metal ions and biomolecules hardly shows the amperometric signal on the biosensor modified electrode. The addition of 50 µM dopamine shows a tiny response, yet the relative potential and response of dopamine are way more positive than the applied potential (-0.2 V) of our study [**45**]. In contrast, good response appeared for 0.5 µM H_2O_2 addition, which suggests the excellent reduction capability of the as-prepared biosensor. It is interesting to note that the amperometric response caused by interfering responses were none or often negligible to compare with the response of H_2O_2. The high anti-interference ability of H_2O_2 on the nanocomposite electrode is mainly associated with the selective reduction capability of Fe^{II}/Fe^{III} redox-active centre on the immobilised hemin. **Fig. 6D** of the MWCNT-CNC/ZnO NR/hemin nanocomposite electrode confirms the excellent operational stability for presence of different concentration (a= 200 µM, a' = 50 µM) of H_2O_2. The strong adsorption of hemin molecule on the MWCNT-CNC/ZnO NR nanocomposite is resulting in excellent operational stability of the biosensor. These results authenticate that the MWCNT-CNC/ZnO NR/hemin nanocomposite electrode can act as a sensitive probe for the real-time electrochemical selective quantification of H_2O_2.

3.5. Determination of H_2O_2 in milk samples

The practical applicability of MWCNT-CNC/ZnO NR/hemin nanocomposite electrode was examined towards the detection of H_2O_2 containing real samples. The real sample analysis was performed using amperometric *i-t* method and the experimental conditions were similar to **Fig. 6A**. First, the impurities from the raw milk were removed by mixing the 20 mL of milk with H_2SO_4 (4:1 ratio) and centrifuged (20 min) using 6000 RPM. The supernatant milk solution was further used as a standard solution and its pH adjured to pH 7.0. The standard addition method is used for the recoveries calculation of H_2O_2 in milk sample [**46**]. The obtained recoveries of H_2O_2 are the obtained recoveries were summarised in **Table 2**. From **Table 2**, one can easily see that the MWCNT-CNC/ZnO NR/hemin nanocomposite electrode has 97.8% recovery of

H_2O_2 in low-fat milk samples. Thus, the MWCNT-CNC/ZnO NR/hemin nanocomposite biosensor can put forward into the real-time application for monitoring of H_2O_2 in food samples.

4. Conclusion

In conclusion, we have developed a stable and sensitive H_2O_2 biosensor using MWCNT-CNC/ZnO NR/hemin composite for the first time. A simple solution-based sonochemical route has been used for the synthesis of ZnO NR on MWCNT-CNC nanocomposite. The formation of MWCNT-CNC/ZnO NR/hemin nanocomposite has been confirmed by a number of physicochemical methods. The UV-Vis spectroscopy and cyclic voltammetry results confirmed the successful immobilisation of hemin on as-synthesized the nanocomposite. The proposed biosensor displayed an excellent catalytic activity and lower reduction potential towards H_2O_2 than other hemin modified biosensors. Also, the biosensor showed a more extensive linear response range (up to 4.18 mM) and lower LOD (4 nM) for the detection of H_2O_2. The biosensor offered excellent selectivity towards H_2O_2 in the presence of a range of potentially active interfering compounds. The MWCNT-CNC/ZnO NR/hemin nanocomposite had appropriate recovery of H_2O_2 in milk samples which authenticates the potential ability of the as-prepared biosensor for future practical applications.

5. Conflicts of interest

We do not have any competing interests to declare.

Acknowledgement

Authors express sincere thanks to the Center of Precision Analysis and Material Research, National Taipei University of Technology for providing the all necessary Instrument facilities. Dr Selvakumar Palanisamy acknowledges the National Taipei University of Technology for the post-doctoral fellowship.

References

[1] C. Chen, Q. Xie, D. Yang, H. Xiao, Y. Fu, Y. Tan, S. Yao, Recent advances in electrochemical glucose biosensors: a review. RSC Adv., 3 (2013) 4473-4491.

[2] Y. Shao, J. Wang, H. Wu, J. Liu, I.A. Aksay, Y. Lin, Graphene Based Electrochemical Sensors and Biosensors: A Review, Electroanalysis 22 (2010) 1027–1036.

[3] B.E. Watt, A.T. Proudfoot, J.A. Vale, Hydrogen peroxide poisoning. Toxicol. Rev. 23 (2004) 51–57.

[4] H.C. Ding, L. Zhang, Z.R. Tang, Y.P. Dong, X.F. Chu, Black phosphorus quantum dots doped ZnO nanoparticles as efficient electrode materials for sensitive hydrogen peroxide detection. J. Electroanal. Chem. 824 (2018) 161–168.

[5] T. Selvaraju, R. Ramaraj, Electrocatalytic reduction of hydrogen peroxide at nanostructured copper modified electrode. J. Appl. Electrochem. 39 (2009) 321-327.

[6] X. Han, C, Tian, M.S. Yuan, Z. Li, W. Wang, T. Li, S.W. Chen, J. Wang, Colorimetric hydrazine detection and fluorescent hydrogen peroxide imaging by using a multifunctional chemical probe, Anal. Chim. Acta. 1052 (2019) 137-144.

[7] M. Wang, D. Wang, S. Qiu, J.X. Huahua, C.J. Zou, Multi-wavelength spectrophotometric determination of hydrogen peroxide in water by oxidative coloration of ABTS via Fenton reaction. Environ. Pollut. Res. 26 (2019) 27063–27072.

[8] M.J. Song, S.W. Hwang, D Whang, Non-enzymatic electrochemical CuO nanoflowers sensor for hydrogen peroxide detection. Talanta 80 (2010) 1648–1652.

[9] H.C. Ding, L. Zhang, Z.R. Tang, Y.P. Dong, X.F. Chu, Black phosphorus quantum dots doped ZnO nanoparticles as efficient electrode materials for sensitive hydrogen peroxide detection. J. Electroanal. Chem. 824 (2018) 161–168.

[10] S. Chen, R. Yuan, Y. Chai, F. Hu, Electrochemical sensing of hydrogen peroxide using metal nanoparticles: a review, Microchim. Acta. 180 (2013) 15–32.

[11] A.S. Rad, A. Mirabi, E. Binaian, H. Tayebi, A Review on Glucose and Hydrogen Peroxide Biosensor Based on Modified Electrode Included Silver Nanoparticles. Int. J. Electrochem. Sci., 6 (2011) 3671 – 3683.

[12] K. Dhar, D.R. Mahapatra, Recent advances in electrochemical nonenzymatic hydrogen peroxide sensors based on nanomaterials: a review. J. Mater. Sci. 54 (2019) 12319–12357.

[13] W. Huang, Q. Hao, W. Lei, L. Wu, X. Xia, Polypyrrole-hemin-reduce graphene oxide: rapid synthesis and enhanced electrocatalytic activity towards the reduction of hydrogen peroxide. Mater. Res. Express. 1 (2014) 045601.

[14] X. Li, G. Luo, H. Xie, Y. Niu, X. Li, R. Zou, Y. Xi, Y. Xiong, W. Sun, G. Li, Voltammetric sensing performances of a carbon ionic liquid electrode modified with black phosphorene and hemin. Microchim. Acta. 186 (2019) 304.

[15] B. Wang, X. Ji, J. Ren, R. Ni, L. Wang, Enhanced electrocatalytic activity of graphene-gold nanoparticles hybrids for peroxynitrite electrochemical detection on hemin-based electrode. Bioelectrochemistry 118 (2017) 75–82.

[16] F.Y. Kong, W.W. Li, J.Y. Wang, H.L. Fang, D.H. Fan, W. Wang, Direct electrolytic exfoliation of graphite with hemin and single-walled carbon nanotube: Creating functional hybrid nanomaterial for hydrogen peroxide detection. Anal. Chim. Acta. 884 (2015) 37–43.

[17] M. Zhang, Z. Huang, G. Zhou, L. Zhu, Y. Feng, T. Lin, H. Hou, Q. Guo, A sensitive hydrogen peroxide sensor based on a three-dimensional N-doped carbon nanotube hemin modified electrode. Anal. Methods. 7 (2015) 8439–8444.

[18] J. Wang, Carbon-Nanotube Based Electrochemical Biosensors: A Review. Electroanalysis. 17 (2005) 7–14.

[19] Y.J. Lee, S.R. Ham, J.H. Kim, T.H. Yoo, S.R. Kim, Y.T. Lee, D.K Hwang, B. Angadi, W.S. Seo, B.K. Ju, W.K. Choi, Highly dispersible buckled nanospring carbon nanotubes for polymer nano composites. Sci Rep. 8 (2018) 4851.

[20] G. Yellapu C.V. Chachin V. Pramod, K. Madathil, P. Saha, R.R. Bojja, S. Gandham, R. Kanaparthi, Functionalized multi-walled carbon nanotubes based Newtonian Nano fluids for medium temperature heat transfer applications. Thermal Sci. Eng. Prog. 12 (2019) 13-23.

[21] K. Sipa, M. Brycht, A. Leniart, P. Urbaniak, A.N. Wiercińsk, B. Pałecz, S. Skrzypek, β–Cyclodextrins incorporated multi-walled carbon nanotubes modified electrode for the voltammetric determination of the pesticide dichlorophen, Talanta. 176 (2018) 625–634.

[22] Y. Wang, C. Wang, X. Song, S.K. Megarajan, H. Jiang, A facile nanocomposite strategy to fabricate a rGO–MWCNT photothermal layer for efficient water evaporation†, J. Mater. Chem. A. 6 (2018) 963-971.

[23] S. Zhang, F. Zhang, Y. Pan, L. Jin, B. Liu, Y. Mao, J. Huang, Multiwall-carbon-nanotube/cellulose composite fibers with enhanced mechanical and electrical properties by cellulose grafting. RSC Adv., 8 (2018), 5678-5684.

[24] S. Ramesh, Y.J. Lee, S. Msolli, J.G. Kim, H.S. Kim, J.H. Kim, Synthesis of a Co_3O_4@gold/MWCNT/polypyrrole hybrid composite for DMMP detection in chemical sensors, RSC Adv., 7 (2017) 50912-50919.

[25] A. Mandal, D. Chakrabarty, Isolation of nanocellulose from waste sugarcane bagasse (SCB) and its characterization, Carbohydr. Polym.. 86 (2011) 1291– 1299.

[26] J. Tang, J. Sisler, N. Grishkewich, K.C. Tam, Functionalization of cellulose nanocrystals for advanced applications. J. Colloid Interface Sci. 494 (2017) 397–409.

[27] Z.L. Wang, Nanostructures of zinc oxide. Mater. Today. 7 (2004) 26-33.

[28] M.F. Khouzani, Z. Fereshteh, M.R.L. Estarki, R.S. Razavi, Different morphologies of ZnO nanostructures via polymeric complex sol–gel method: synthesis and characterization. J Sol-Gel Sci Technol. (2012) DOI 10.1007/s10971-012-2847-y.

[29] H.A. Wahab, A.A. Salam, A.A.E. Saeid, M. Willander, O. Nur, I.K. Battish, Zinc oxide nano-rods based glucose biosensor devices fabrication. Result. Phy. 9 (2018) 809-814.

[30] H. Xu, B.W. Zeiger, K.S. Suslick, Sonochemical synthesis of nanomaterials, Chem. Soc. Rev., 42 (2013) 2555-2567.

[31] N. Karikalan, M. Elavarasan, T.C.K. Yang, Effect of cavitation erosion in the sonochemical exfoliation of activated graphite for electrocatalysis of acebutolol, Ultrason. Sonochem. 56 (2019) 297-304.

[32] Y. Zhao, X. Fang, X. Yan, X. Zhang, Z. Kang, G. Zhang, Y. Zhang, Nanorod arrays composed of zinc oxide modified with gold nanoparticles and glucose oxidase for enzymatic sensing of glucose. Microchim. Acta. 182 (2015) 605–610.

[33] Y. Zhao, W. Li, L. Pan, D. Zhai, Y. Wang, L. Li, W. Cheng, W. Yin, X. Wang, J.B. Xu, Y. Shi. ZnO-nanorods/graphene heterostructure: a direct electron transfer glucose biosensor. Sci Rep. 6 (2016) 32327.

[34] S. Tiwari, M. Vinchurkar, V.R. Rao, G. Garnier, Zinc oxide nanorods functionalized paper for protein preconcentration in biodiagnostics. Sci Rep. 7 (2017) 43905.

[35] S. Palanisamy, S.M. Chen, R. Sarawathi, A novel nonenzymatic hydrogen peroxide sensor based on reduced graphene oxide/ZnO composite modified electrode, Sensors. Actuators, B, 166 (2012) 372-377.

[36] J.P. Liu, C.X. Guo, C.M. Li, Y.Y. Li, Q.B. Chi, X.T. Huang, L. Liao, T. Yu, Carbon decorated ZnO nanowire array: a novel platform for direct electrochemistry of enzymes and biosensing applications, Electrochem. Commun., 11 (2009) 202-205.

[37] R. Ahmad, N. Tripathy, M.S. Ahn, K.S. Bhat, T. Mahmoudi, Y. Wang, J.Y. Yoo, D.W. Kwon, H.Y. Yang, Y.B. Hahn, Highly efficient non-enzymatic glucose sensor based on CuO modified vertically-grown ZnO nanorods on electrode, Sci Rep. 7 (2017) 5715.

[38] V. Velusamy, S. Palanisamy, S.M. Chen, T.W. Chen, S. Selvam, S.K. Ramaraj, B.S. Lou, Graphene dispersed cellulose microfibers composite for efficient immobilization of hemoglobin and selective biosensor for detection of hydrogen peroxide. Sensors. Actuators, B 252 (2017) 175-182

[39] S. Palanisamy, V. Velusamy, S.W. Chen, T.C.K. Yang, S. Balu, C. E. Banks, Enhanced reversible redox activity of hemin on cellulose microfiber integrated reduced graphene oxide for H_2O_2 biosensor applications. Carbohydr. Polym.. 204 (2019) 152-160.

[40] H. Wu, T. Wei, X. Li, J. Yang, J. Zhang, S. Fan, and H. Zhang, Synergistic-effect-controlled tetraoctylammonium bromide/multi-walled carbon nanotube@hemin hybrid material for construction of electrochemical sensor. J. Electrochem. Soc. 164 (2017) B147-B151.

[41] Y. Guo, J. Li, S. Dong, Hemin functionalized graphene nanosheets-based dual biosensor platforms for hydrogen peroxide and glucose. Sensors. Actuators, B 160 (2011) 295– 300.

[42] W. Wang, H. Tang, Y. Wu, Y. Zhang, Z. Li, Highly electrocatalytic biosensor based on Hemin@AuNPs/reduced graphene oxide/chitosan nanohybrids for non-enzymatic ultrasensitive detection of hydrogen peroxide in living cells. Biosens. Bioelectron. 32 (2019) 217–223.

[43] J. Chen, L. Zhao, H. Bai, G. Shi, Electrochemical detection of dioxygen and hydrogen peroxide by hemin immobilized on chemically converted graphene. J. Electroanal. Chem. 657 (2011) 34–38.

[44] S. Palanisamy, S. Cheemalapati, S.M. Chen, Highly sensitive and selective hydrogen peroxide biosensor based on hemoglobin immobilized at multiwalled carbon nanotubes–zinc oxide composite electrode, Anal. biochem. 429 (2012) 108-115.

[45] S. Balu, S. Palanisamy, V. Velusamy, T.C.K. Yang, E.S.I. El-Shafey, Tin disulfide nanorod-graphene-β-cyclodextrin nanocomposites for sensing dopamine in rat brains and human blood serum, Mater. Sci. Eng., C, 108 (2020) 110367.

[46] S. Balu, S. Palanisamy, V. Velusamy, T.C.K. Yang, Sonochemical synthesis of gum guar biopolymer stabilized copper oxide on exfoliated graphite: Application for enhanced electrochemical detection of H_2O_2 in milk and pharmaceutical samples, Ultrason. Sonochem. 56 (2019) 254-263.

Table captions

Table 1 The comparative results of MWCNT-CNC/ZnO NR/hemin biosensor with various biosensors using hemin and hemoglobin immobilised graphene and multiwalled carbon nanotube composites for the determination of H_2O_2.

Table 2 Determination of H_2O_2 in milk samples using MWCNT-CNC/ZnO NR/hemin biosensor (Relative standard deviation (RSD) related to 3 experiments).

Biosensor electrode	E_{app} (V)	Ks (s^{-1})	Linear range (μM)	LOD (nM)	Ref.
PPY/He-RGO/GCE	-0.15	–	0.5-80.0	130.0	[13]
PEDOT:PSS-CIL-He/GCE	-0.03	1.58	4000–35000.0	1300.0	[14]
NCNTs-He/GCE	-0.15	–	0.08–137.2	30.0	[17]
GN–He–SWCNT/GCE	-0.2	–	0.2–400.0	50.0	[16]
GR-CMF-Hb/GCE	-0.3	6.17	0.05-926.0	10.0	[38]
RGO-CMF-He/GCE	-0.2	6.87	0.06–540.6	16.0	[39]
TOAB/MWCNT@Hemin/GCE	-0.94	–	0.82–278.6	260.0	[40]
GNs-He/GCE	-0.2	–	0.5–400.0	200.0	[41]
He@AuNPs/RGO/CHI/GCE	-0.3	–	1.0–1000.0	9.3	[42]
CCGR-He/GCE	-0.2	–	1-3000.0	350.0	[43]
MWCNT-ZnO-Hb/GCE	-0.34	1.26	0.1–36.6	20.0	[44]
MWCNT-CNC/ZnO NR/He/SPCE	-0.2	6.96	0.01–4183.3	4.0	This work

Table 1

Real sample	Added H_2O_2 (μM)	Found H_2O_2 (μM)	Recovery (%)	RSD (%)
Milk (low-fat)	1.0	0.98	98.0	3.1
	2.9	2.81	96.9	5.6
	5.8	5.72	98.6	3.9

Table 2

Figure captions

Scheme 1 Pictorial depiction for the solution based sonochemical synthesis of ZnO and MWCNT-CNC/ZnO NR composite and fabrication of the MWCNT-CNC/ZnO NR/hemin biosensor.

Figure 1 FESEM images of MWCNT (A), CNC (B), CMF (inset), MWCNT-CNC (C), CNC/ZnO NR (D), MWCNT-CNC/ZnO NR (E) and MWCNT-CNC/ZnO NR/hemin (F). G) EDS of the MWCNT-CNC/ZnO NR/hemin composite.

Figure 2 A) XRD pattern of MWCNT (a), CNC/ZnO NR (b) and MWCNT-CNC/ZnO NR/hemin (c). B) FTIR spectra of MWCNT (a), MWCNT-CNC (b), MWCNT-CNC/ZnO NR (c) and MWCNT-CNC/ZnO NR/hemin (d). C) Raman spectra of the MWCNT (a), MWCNT-CNC (b) and MWCNT-CNC/ZnO NR (c). D) Typical UV-Vis spectra of ZnO NR (a), MWCNT (b), MWCNT-CNC/ZnO NR/hemin (c) and pristine hemin (d).

Figure 3 A) Cyclic voltammogram obtained for hemin immobilized different modified SPCEs, hemin/SPCE (a), CNC/ZnO NR/hemin/SPCE (b), MWCNT/hemin/SPCE (c), MWCNT-CNC/hemin/SPCE (d) and MWCNT-CNC/ZnO NR/hemin/SPCE (e) in a deoxygenated pH 7.0 at a scan rate of 100 mV/s. At the same conditions, MWCNT-CNC/ZnO NR modified SPCE in the absence of hemin (a'). B) Cyclic voltammetric response and the electron transfer characteristics of MWCNT-CNC/ZnO NR, CNC/ZnO, MWCNT-CNC and pristine MWCNT modified SPCEs in 5 mM potassium ferricyanide containing 0.1 M KCl.

Figure 4 A) Cyclic voltammetric response obtained for MWCNT-CNC/ZnO NR/hemin/SPCE in a deoxygenated pH 7.0 at a different scan rate (50–500 mV/s). B) Plot for scan rate vs. I_{pa} and I_{pc} of hemin redox couple. C) Cyclic voltammetric response of MWCNT-CNC/ZnO NR/hemin modified SPCE in deoxygenated various pH at a scan rate of 100 mV/s. D) Linear plot of E_{pa} and E_{pc} of hemin redox couple vs pH.

Figure 5 A) Cyclic voltammetric response of hemin/SPCE (a), CNC/ZnO NR/hemin/SPCE (b), MWCNT-CNC/hemin/SPCE (c) and MWCNT-CNC/ZnO NR/hemin/SPCE (d) in a deoxygenated pH 7.0 containing 1.2 mM H_2O_2 at a scan rate of 100 mV/s. B) The related cathodic current response and reduction potential of H_2O_2 on hemin immobilised different modified SPCEs. C) Cyclic voltammetric response of MWCNT-CNC/ZnO NR/hemin modified SPCE in the absence (a') and presence of 0.2 mM (a), 0.7 mM (b) and 1.2 mM H_2O_2 containing deoxygenated pH 7.0 at a scan rate of 100 mV/s. D) Linear plot of E_{pc} vs $[H_2O_2]$.

Scheme 2 The mechanism for the electrocatalytic reduction of H_2O_2 and redox electrochemistry of immobilised hemin on MWCNT-CNC/ZnO NR nanocomposite.

Figure 6 A) Real-time amperometric current response of MWCNT-CNC/ZnO NR/hemin/SPCE for the addition of H_2O_2 into the constantly stirred (750 RPM) deoxygenated pH 7.0. E_{app} = -0.2 V. Inset shows the enlarged amperometric current response view for the addition of 0.01 (a), 0.1 (b), 1.0 (c), 5.0 (d), 25.0 (e), 75.0 (f) and 150 µM (g) H_2O_2. B) Calibration plot for the amperometric current response vs [H_2O_2]. C) The amperometric response for the effect of the addition of 0.5 µM H_2O_2 (a) and 50 µM of potentially interfering different electroactive compounds (b-n) into the constantly stirred deoxygenated pH 7.0 at an E_{app} of -0.2 V. D) Operational stability of the fabricated biosensor.

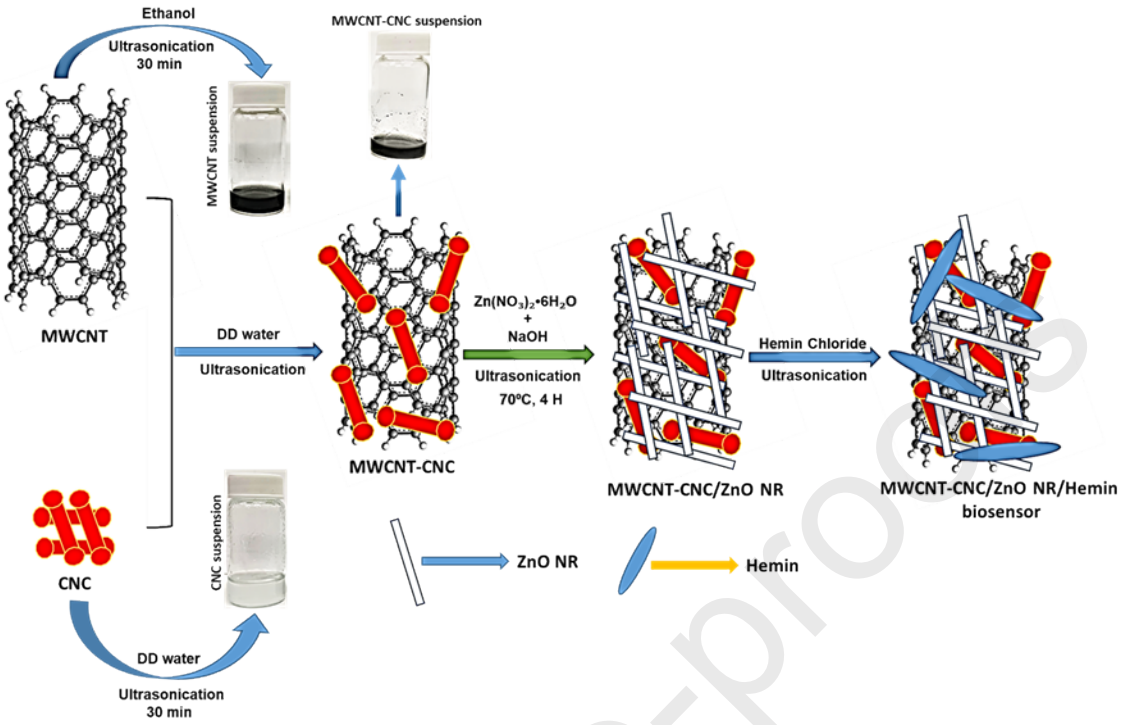

Scheme 1

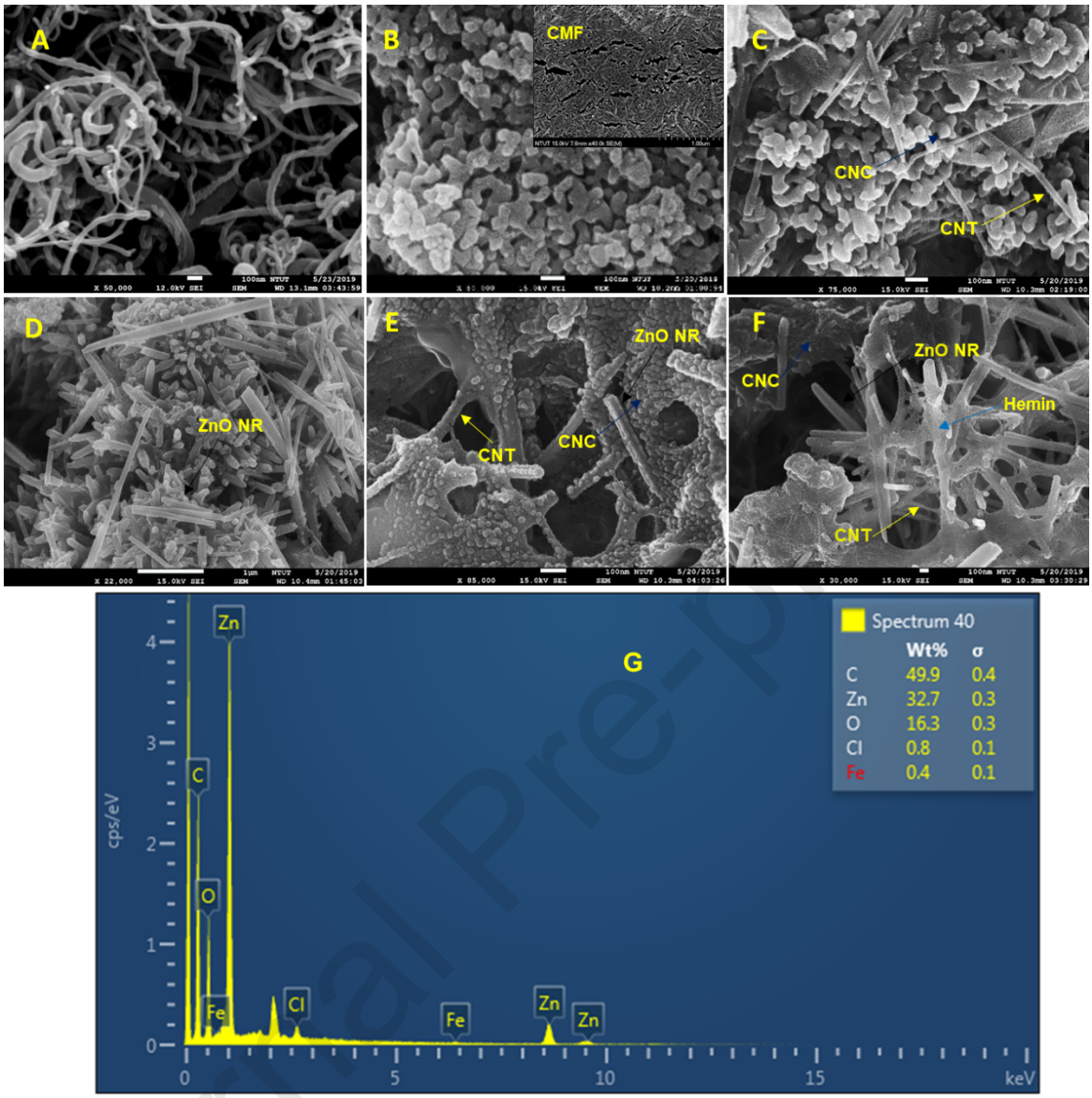

Figure 1

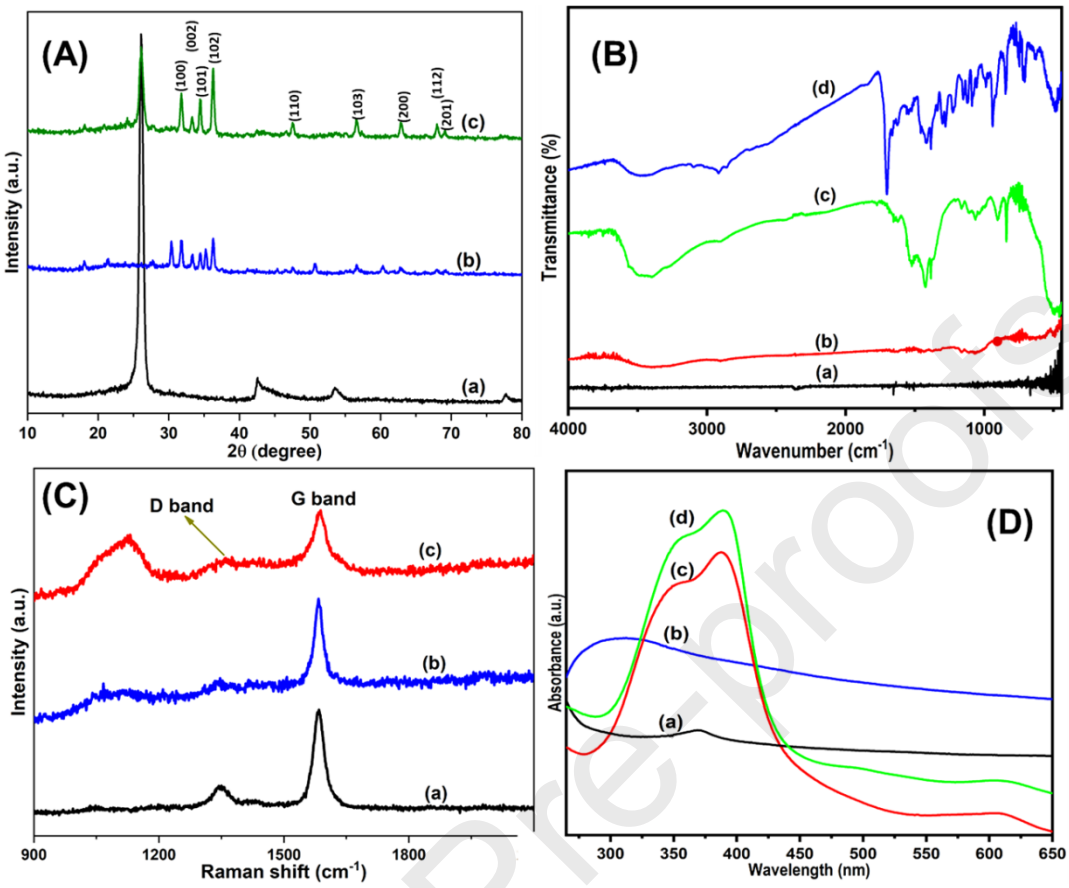

Figure 2

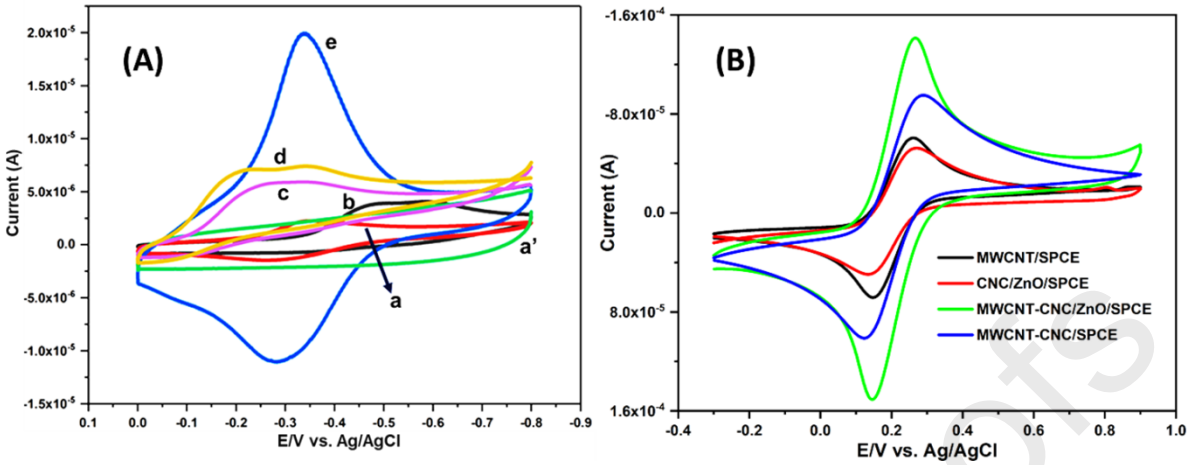

Figure 3

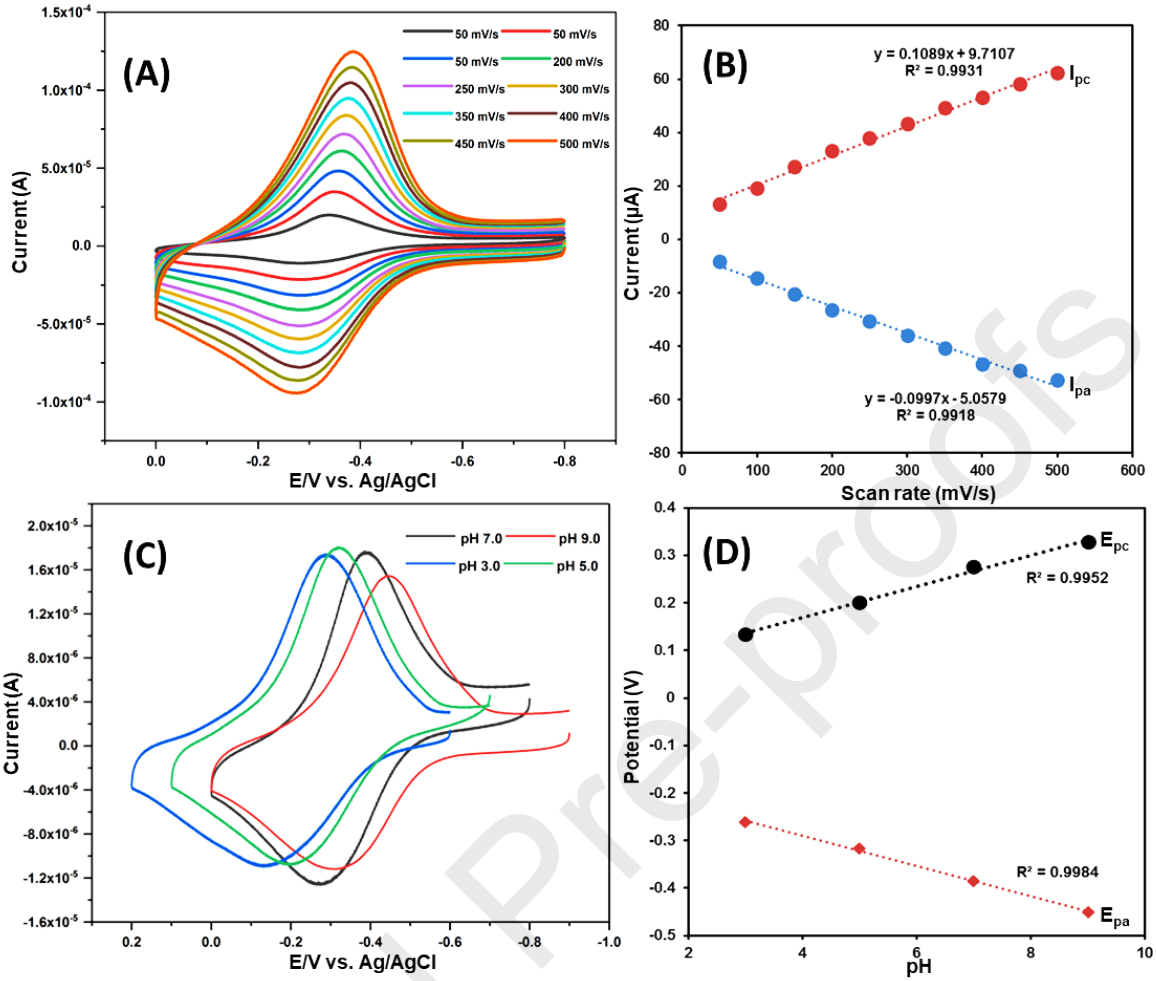

Figure 4

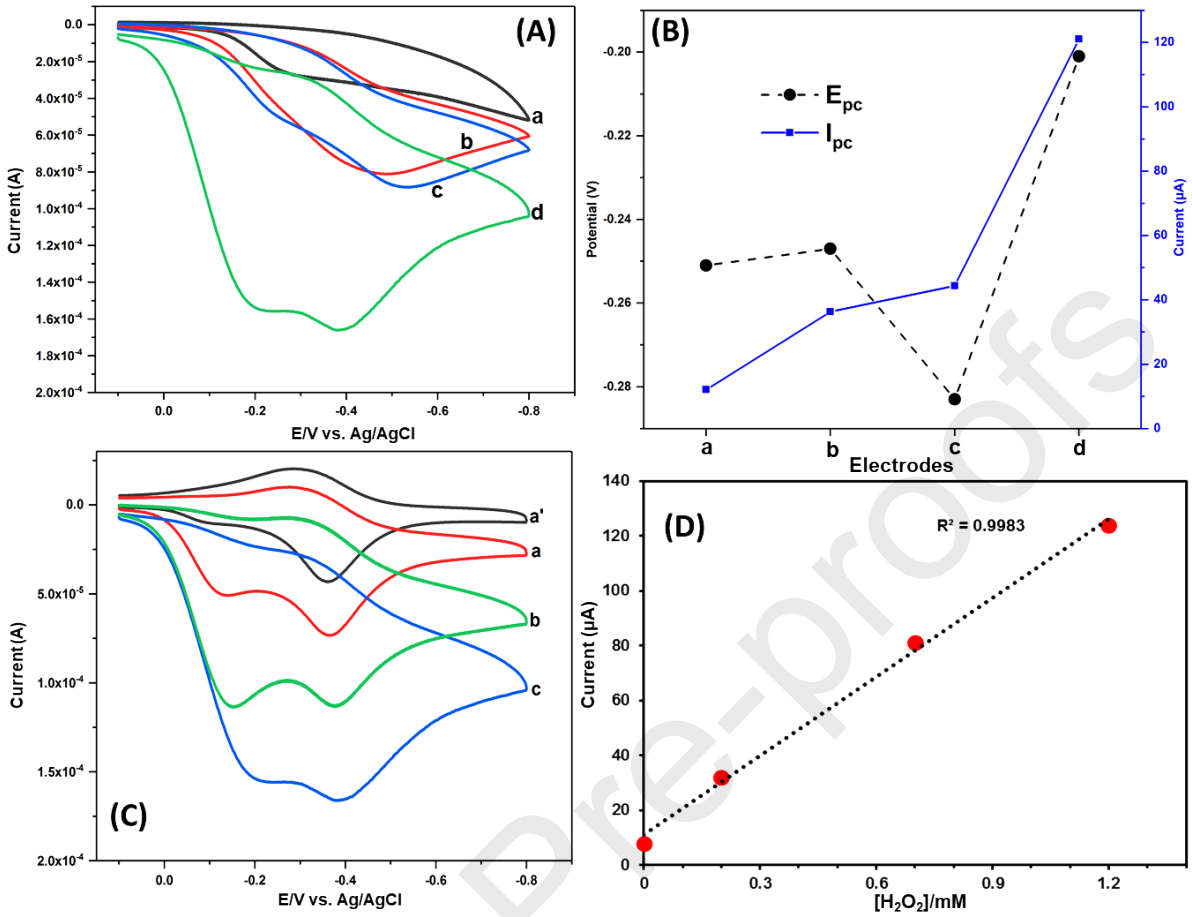

Figure 5

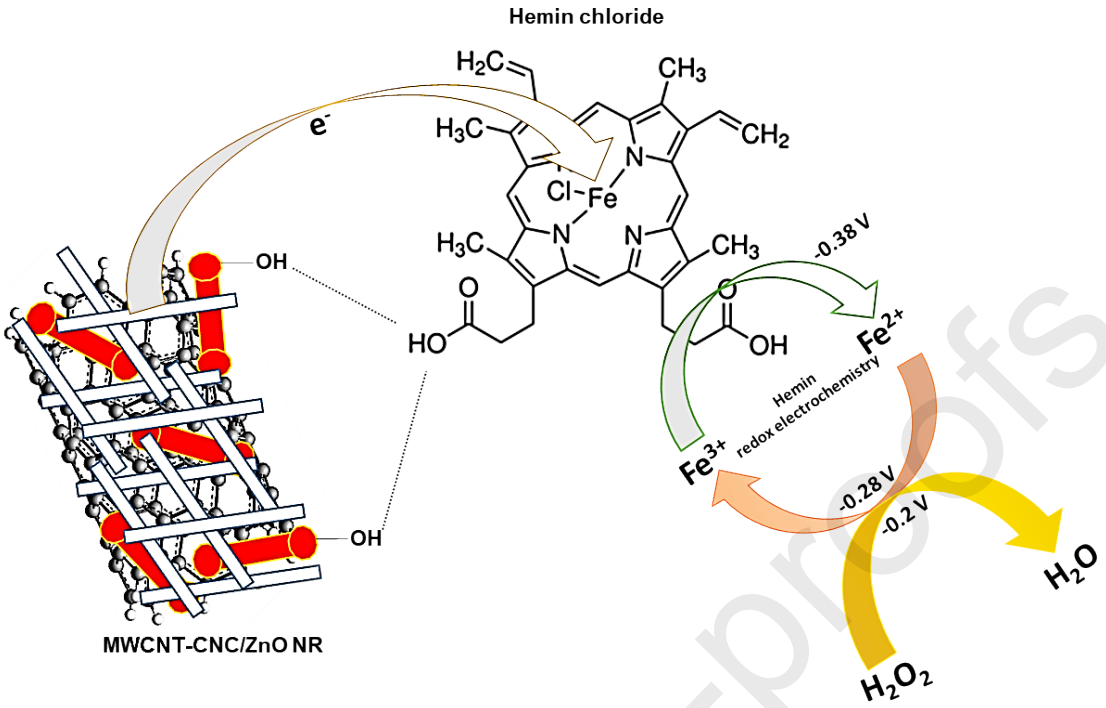

Scheme 2

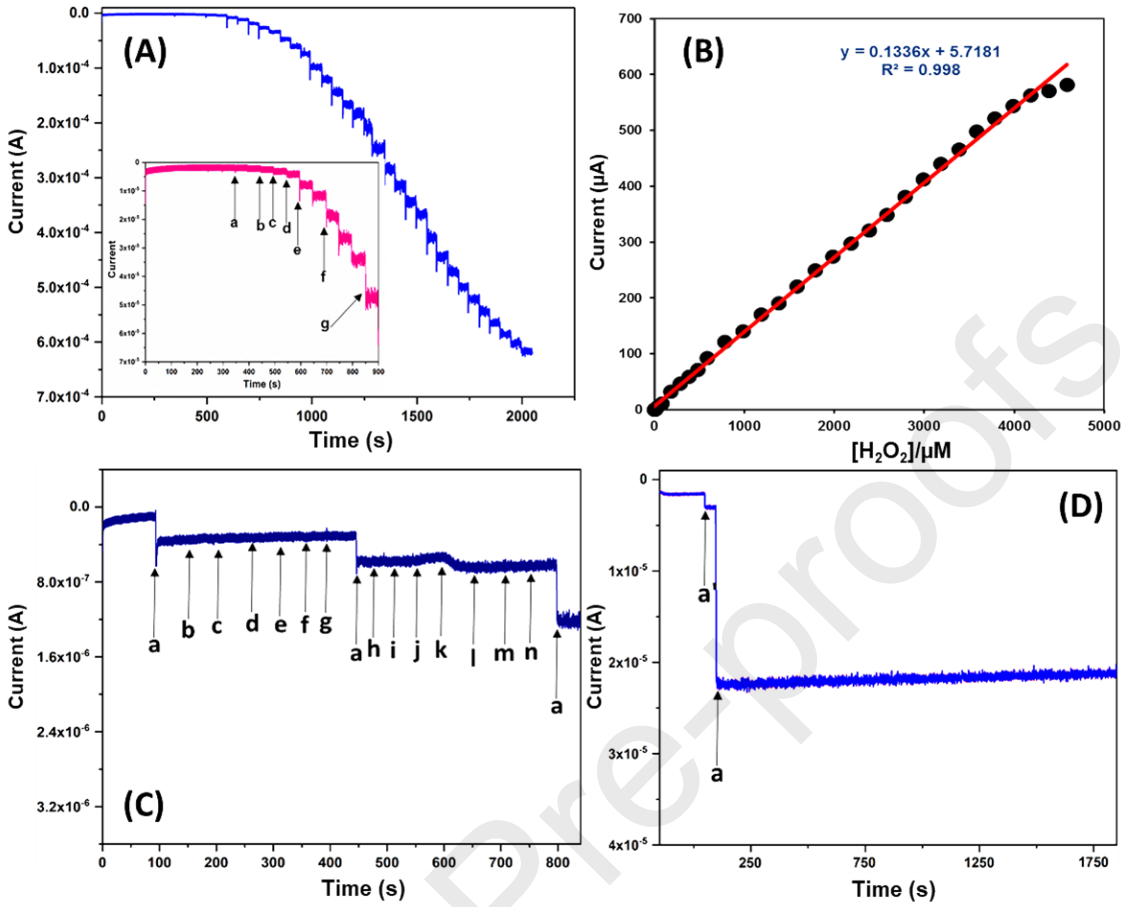

Figure 6

Graphics for manuscript

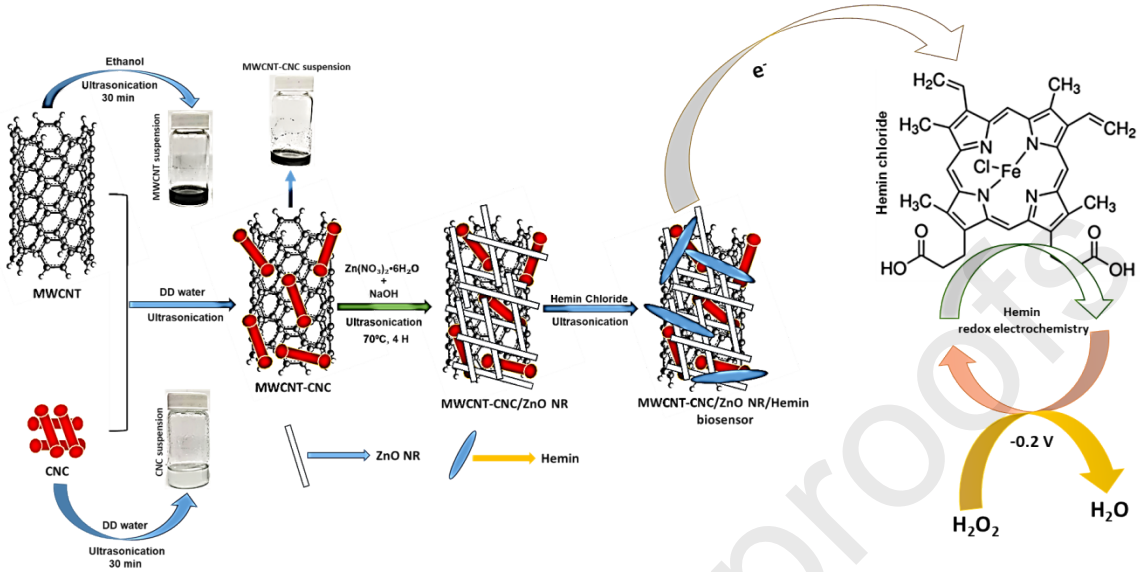

Highlights

- A simple sonochemical method has been adopted for the preparation of MWCNT-CNC nanocomposite.
- The ZnO NR on MWCNT-CNC nanocomposite has been prepared using a solution based sonochemical approach for the first time.
- The MWCNT-CNC/ZnO NR nanocomposite has been used as immobilisation matrix for hemin and construction of H_2O_2 biosensor.
- A lower LOD of 4.0 nM with lower reduction potential of H_2O_2 has been achieved using MWCNT-CNC/ZnO NR/hemin biosensor.
- The practicality of the fabricated biosensor has been validated in milk samples.

Conflicts of interest

We do not have any known competing interests to declare.